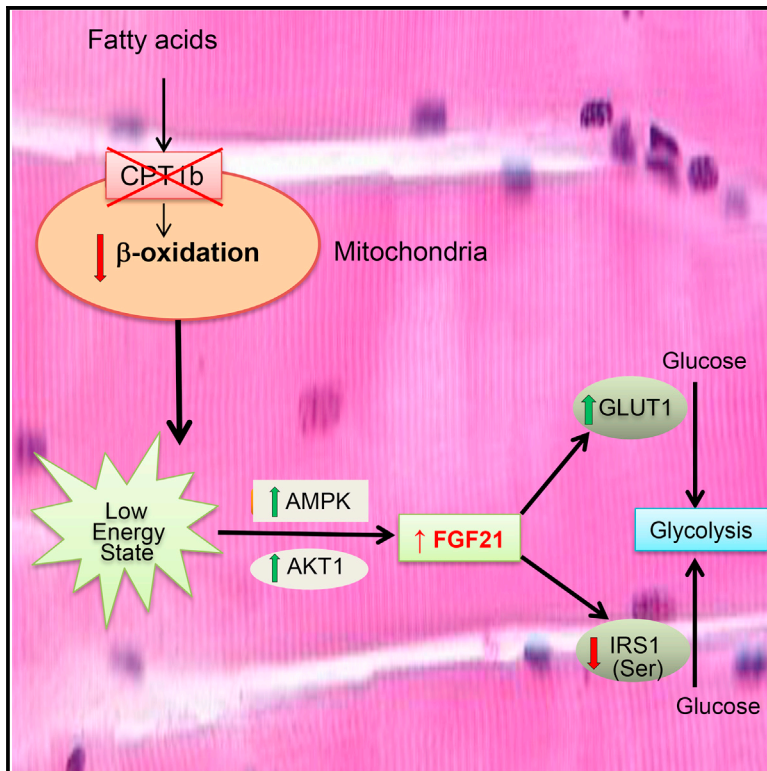


Impaired Mitochondrial Fat Oxidation Induces FGF21 in Muscle

Graphical Abstract



Authors

Bolormaa Vandanmagsar,
Jaycob D. Warfel, Shawna E. Wicks, ...,
Jingying Zhang, Robert C. Noland,
Randall L. Mynatt

Correspondence

randall.mynatt@pbrc.edu

In Brief

Vandanmagsar et al. show that inhibition of mitochondrial fatty acid oxidation in muscle results in a local increase in FGF21 that is dependent on AMPK and Akt1 signaling but independent of the stress signaling pathways. FGF21 acts in a paracrine manner to increase glucose uptake in muscle.

Highlights

- Decreased muscle fat oxidation (FAO) increases glucose uptake and decreases fat mass
- Decreased FAO creates a starvation response, inducing FGF21 specifically in muscle
- FGF21 acts in a paracrine manner to increase glucose uptake in muscle
- FGF21 does not contribute to decreased fat mass



Impaired Mitochondrial Fat Oxidation Induces FGF21 in Muscle

Bolormaa Vandanmagsar,¹ Jaycob D. Warfel,¹ Shawna E. Wicks,¹ Sujoy Ghosh,^{6,7} J. Michael Salbaum,² David Burk,³ Olga S. Dubuisson,¹ Tamra M. Mendoza,¹ Jingying Zhang,⁴ Robert C. Noland,⁵ and Randall L. Mynatt^{1,4,*}

¹Gene Nutrient Interactions Laboratory

²Genomics Core Facility

³Cell Biology and Bioimaging Core Facility

⁴Transgenic Core Facility

⁵Skeletal Muscle Metabolism Laboratory

⁶Computational Biology Laboratory

Pennington Biomedical Research Center, Louisiana State University, Baton Rouge, LA 70808, USA

⁷Centre for Computational Biology and Program in Cardiovascular and Metabolic Disorders, Duke-NUS Graduate Medical School, Singapore 169857, Singapore

*Correspondence: randall.mynatt@pbrc.edu

<http://dx.doi.org/10.1016/j.celrep.2016.04.057>

SUMMARY

Fatty acids are the primary fuel source for skeletal muscle during most of our daily activities, and impaired fatty acid oxidation (FAO) is associated with insulin resistance. We have developed a mouse model of impaired FAO by deleting carnitine palmitoyltransferase-1b specifically in skeletal muscle (*Cpt1b*^{m-/-}). *Cpt1b*^{m-/-} mice have increased glucose utilization and are resistant to diet-induced obesity. Here, we show that inhibition of mitochondrial FAO induces FGF21 expression specifically in skeletal muscle. The induction of FGF21 in *Cpt1b*-deficient muscle is dependent on AMPK and Akt1 signaling but independent of the stress signaling pathways. FGF21 appears to act in a paracrine manner to increase glucose uptake under low insulin conditions, but it does not contribute to the resistance to diet-induced obesity.

INTRODUCTION

Fat contributes 90% of the substrate for resting energy expenditure in skeletal muscle and remains the primary fuel during daily activities and low exercise intensities (<40% VO₂ max) (Brooks, 1997; Brooks and Mercier, 1994; Dagenais et al., 1976; Kelley et al., 1993). Carnitine palmitoyltransferase-1 (CPT1) is located on the outer mitochondrial membrane and transports long-chain fatty acids into mitochondria for β -oxidation. We created a mouse model of impaired fatty acid oxidation (FAO) by deleting CPT1b in skeletal muscle (*Cpt1b*^{m-/-}) and reported that inhibition of mitochondrial FAO leads to activation of AMPK and PGC1 α , resulting in adaptive metabolic responses in skeletal muscle with increased mitochondrial biogenesis, oxidative capacity, compensatory peroxisomal fat oxidation, and amino acid catabolism (Wicks

et al., 2015). In addition, despite elevated plasma lipids and accumulation of both intramyocellular lipids and lipotoxic species, fasting insulin and glucose are lower in *Cpt1b*^{m-/-} mice, with enhanced glucose utilization in *Cpt1b*^{m-/-} mice. Here we report what appears to be a local starvation response in which FGF21 is specifically upregulated in skeletal muscle of *Cpt1b*^{m-/-} mice.

FGF21 was identified as a novel member of the FGF family that is highly expressed in liver (Nishimura et al., 2000). FGF21 was subsequently shown to be a potent metabolic regulator of glucose uptake in adipocytes (Kharitonov et al., 2005) and is generally thought of as a secreted protein produced by liver in response to starvation (Badman et al., 2007; Inagaki et al., 2007). However, under myopathic conditions resulting from deficiencies in the mitochondrial respiratory chain, FGF21 can be secreted from skeletal muscle (Kim et al., 2013b; Tyynismaa et al., 2010). In addition, the transgenic overexpression of Akt1 (Izumiya et al., 2008), perilipin 5 (Harris et al., 2015), and UCP1 (Keipert et al., 2014; Ost et al., 2015) in skeletal muscle induces FGF21 secretion. The skeletal muscle-specific ablation of autophagy-related 7 leads to an autophagy deficiency and mitochondrial dysfunction and increases FGF21 in muscle (Kim et al., 2013b; Tyynismaa et al., 2010). In addition, the skeletal muscle-specific ablation of tuberous sclerosis complex (Tsc) 1, causing activation of mTORC1, induces FGF21 secretion from muscle (Guridi et al., 2015). A common link among these mouse models (except Akt1 overexpression) is metabolic dysfunction, endoplasmic reticulum (ER) stress, and activation of activating transcription factor 4 (Atf4) as a master regulator of the integrative stress response leading to FGF21 induction.

In the present study, we address whether upregulation of FGF21 in skeletal muscle contributes to the enhanced carbohydrate metabolism (improved insulin sensitivity and glucose utilization) in response to inhibition of mitochondrial FAO in *Cpt1b*^{m-/-} mice. We demonstrate that FGF21 can be upregulated by restricting FAO in muscle in an AMPK-Akt1-dependent manner without activation of the integrative stress response. We also determine the role of FGF21 in the overall phenotype of

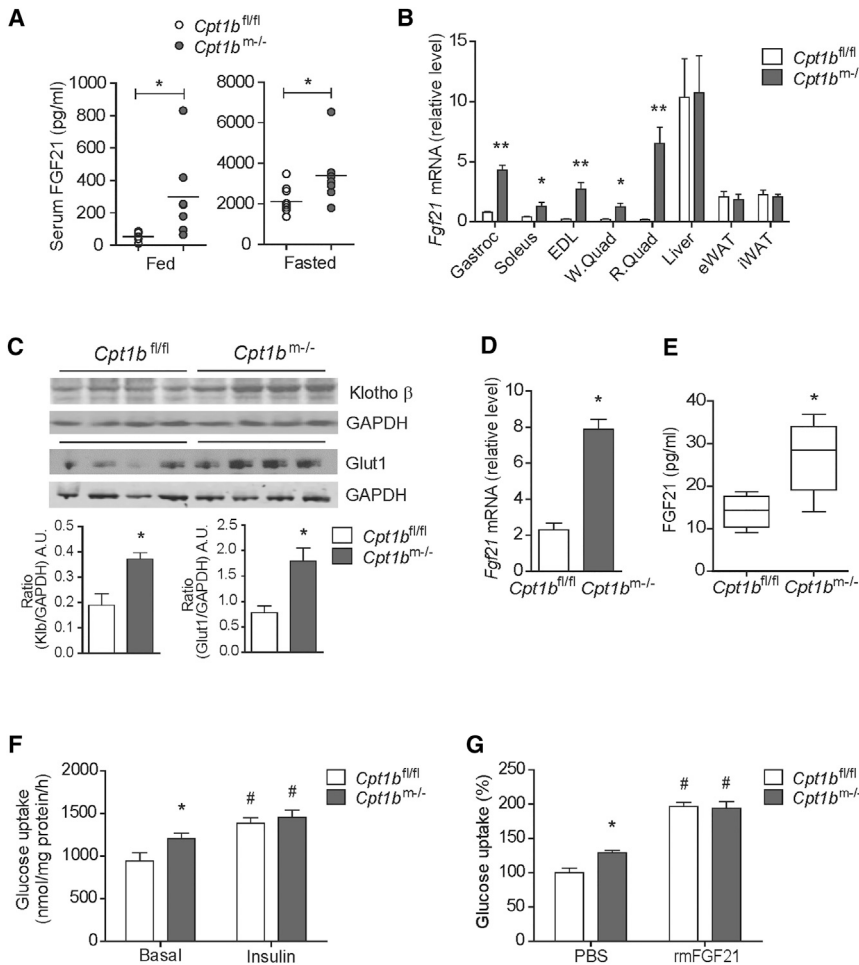


Figure 1. Muscle-Derived FGF21 Enhances Glucose Uptake in Skeletal Muscle in *Cpt1b*^{m-/} Mice

(A) Serum FGF21 concentration in 4-month-old *Cpt1b*^{m-/} and *Cpt1b*^{fl/fl} mice fed and fasted overnight (n = 7–9 per group).

(B) *Fgf21* gene expression in muscle tissue such as gastrocnemius (Gastroc), soleus, extensor digitorum longus (EDL), white and red quads (W.Quad and R.Quad), and other tissue, such as liver, eWAT, and iWAT, from 3- to 5-month-old *Cpt1b*^{m-/} and *Cpt1b*^{fl/fl} mice (n = 5–8).

(C) Immunoblot analysis showing β-Klotho and Glut1 protein abundance in gastrocnemius muscle from 4-month-old *Cpt1b*^{m-/} and *Cpt1b*^{fl/fl} mice. GAPDH was used as a loading control. Imaged software was used for densitometry quantification of the immunoblots. Results shown are representative of three separate experiments (n = 3–4 per group).

(D) *Fgf21* gene expression primary myotubes established from *Cpt1b*^{m-/} and *Cpt1b*^{fl/fl} mice.

(E) Secreted FGF21 over 24 hr in culture media from primary myotubes initiated from *Cpt1b*^{m-/} and *Cpt1b*^{fl/fl} mice.

(F) Basal and insulin-stimulated [³H]-2-deoxyglucose uptake in primary myotubes from *Cpt1b*^{m-/} and *Cpt1b*^{fl/fl} mice.

(G) Primary myotubes from *Cpt1b*^{m-/} and *Cpt1b*^{fl/fl} mice (3–5 months of age) were pre-treated with vehicle (PBS) or rmFGF21 (250 ng/ml, 16 hr), and then [³H]-2-deoxyglucose uptake was measured. Results shown are representative of four independent experiments.

All data are presented as mean ± SEM. *p < 0.05 and **p < 0.01 between *Cpt1b*^{m-/} and *Cpt1b*^{fl/fl} mice, and #p < 0.05 between vehicle and insulin or rmFGF21 treatments.

Cpt1b^{m-/} mice using CPT1b and FGF21 double knockout mice (DKO).

RESULTS

Mitochondrial FAO Deficiency in Muscle Induces FGF21

Serum FGF21 levels were significantly higher in both fed and fasted states in *Cpt1b*^{m-/} mice compared to control mice (Figure 1A). To determine whether increased FGF21 in circulation was arising partly from skeletal muscle, we examined *Fgf21* gene expression in several tissues. The mRNA expression of *Fgf21* was markedly upregulated in several muscles of *Cpt1b*^{m-/} mice compared to *Cpt1b*^{fl/fl} mice, without changes in liver or white adipose tissue (WAT) (Figure 1B).

We next evaluated the effect of muscle-specific upregulation of FGF21 on glucose uptake in skeletal muscle. Gene expression of *Fgfr1* and its spliced variants *Fgfr1b* and *Fgfr1c* were not different in skeletal muscle between *Cpt1b*^{m-/} and control mice (Figures S1A–S1C). However, proteomic (Wicks et al., 2015) and immunoblot analyses of muscle from *Cpt1b*^{m-/} mice revealed significantly elevated protein expression of β-Klotho in muscle, which is the essential co-receptor for FGF21 (Figure 1C) (Ogawa et al., 2007). Consistent with reports that FGF21

increases glucose uptake via glucose transporter 1 (Glut1) (Kharitonov et al., 2005; Mashili et al., 2011), protein expression of Glut1 was markedly increased in muscle of *Cpt1b*^{m-/} mice compared to controls (Figure 1C).

Primary myotubes from *Cpt1b*^{m-/} mice have a metabolic gene expression profile similar to that in muscle from *Cpt1b*^{m-/} mice (Figures S1D and S1E). We found significantly increased mRNA expression and protein secretion of FGF21 in primary myotubes derived from *Cpt1b*^{m-/} mice compared to *Cpt1b*^{fl/fl} mice (Figures 1D and 1E). Basal glucose uptake was significantly elevated in primary myotubes from *Cpt1b*^{m-/} mice; however, insulin-stimulated glucose uptake was comparable to *Cpt1b*^{fl/fl} mice (Figure 1F). FGF21 treatment significantly increased glucose uptake in myotubes from both *Cpt1b*^{m-/} and control mice, suggesting the elevated basal glucose uptake in myotubes from *Cpt1b*^{m-/} mice is potentially a result from enhanced FGF21 production (Figure 1G).

Insulin Sensitivity in *Cpt1b*-Deficient Muscle Is Maintained through mTOR-Akt Signaling

To determine the underlying molecular mechanisms of increased glucose utilization despite lipotoxicity in *Cpt1b*^{m-/} mice, we first examined the mTOR signaling pathway, which senses nutrient

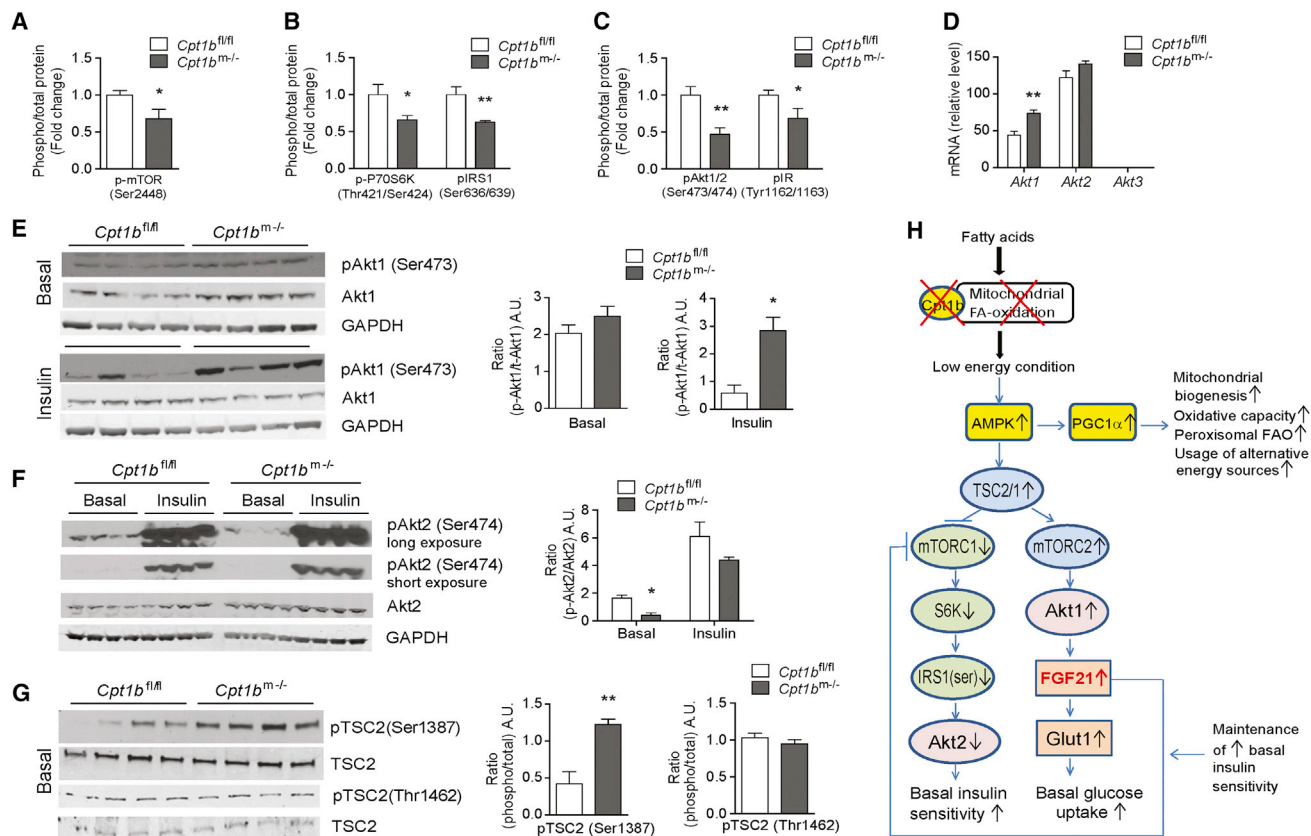


Figure 2. mTOR-Akt Signaling Pathways Are Involved in Induction of *Fgf21* in an Energy-Deficient Condition Caused by Impaired Mitochondrial FAO

(A and B) Activity of mTOR (A) and downstream members of the mTORC1 signaling pathway, P70S6K and IRS1 (B), in gastrocnemius muscle from *Cpt1b^{m-/m-}* and *Cpt1b^{fl/fl}* mice.

(C) Akt and IR signaling at baseline in gastrocnemius muscle from *Cpt1b^{m-/m-}* and *Cpt1b^{fl/fl}* mice.

(D) Gene expression of Akt signaling members, *Akt1*, *Akt2*, and *Akt3* in gastrocnemius muscle from *Cpt1b^{m-/m-}* and *Cpt1b^{fl/fl}* mice (n = 8).

(E and F) Immunoblot analysis of basal and insulin-stimulated Akt1 (E) and Akt2 (F) signaling by phosphorylation at Ser473 and Ser 474, respectively, in red quad muscle from *Cpt1b^{m-/m-}* and *Cpt1b^{fl/fl}* mice. GAPDH was used as a loading control. ImageJ software was used for densitometry quantification of the immunoblots.

(G) Activation of TSC2, as examined by phosphorylation at Ser1387 and Thr1462, in red quad muscle from *Cpt1b^{m-/m-}* and *Cpt1b^{fl/fl}* mice. Results shown are representative of three independent experiments (n = 4 per group).

(H) Proposed model explaining mechanisms of interplay of the AMPK, mTOR, and Akt signaling pathways in the FGF21 induction and enhanced glucose utilization in the condition with mitochondrial FAO deficiency.

All data are presented as mean ± SEM. *p < 0.05 and **p < 0.01.

and energy levels and integrates upstream and downstream signals, including growth factors such as insulin (Wullschlegel et al., 2006). Phosphorylation of mTOR at Ser2448, the site associated with mTORC1 activity (Chiang and Abraham, 2005), was significantly decreased in muscle of *Cpt1b^{m-/m-}* mice compared to *Cpt1b^{fl/fl}* mice (Figure 2A). Likewise, phosphorylation of P70 isoform of S6K1, the main downstream effector of mTORC1 (Wullschlegel et al., 2006), was significantly reduced in skeletal muscle from *Cpt1b^{m-/m-}* mice (Figure 2B). Activation of mTORC1 negatively regulates insulin sensitivity via activation of S6K1, which inhibits IRS protein responsiveness to insulin stimulation by directly phosphorylating IRS1 at Ser636/639 (Um et al., 2004; Wullschlegel et al., 2006). In *Cpt1b^{m-/m-}* skeletal muscle, serine phosphorylation of IRS1 was significantly decreased, suggesting reduced mTORC1 signaling (Figure 2B). In addition, tyrosine

phosphorylation of IRS1, which facilitates insulin responsiveness (Copps and White, 2012), is significantly increased in skeletal muscle of *Cpt1b^{m-/m-}* mice compared to control mice (Figure S2A). As a consequence of decreased inhibitory action of mTORC1 signaling in *Cpt1b^{m-/m-}* muscle in the basal state, we detected significant reductions in basal phosphorylation of both Akt (Ser473) and insulin receptor (IR) (Tyr1162/1163) in skeletal muscle using multiplex and immunoblot analysis (Figures 2C and S2B). Based upon this evidence we predicted that reduced mTORC1 signaling in the basal state would not only improve basal glucose clearance but also increase sensitivity of *Cpt1b^{m-/m-}* muscle to insulin stimulation. Consistent with this, fasting plasma insulin levels were decreased in *Cpt1b^{m-/m-}* mice and remained significantly lower throughout life (Wicks et al., 2015). However, insulin-stimulated phosphorylation of

total Akt (Ser473) was comparable between *Cpt1b*^{m^{-/-}} and control mice (Wicks et al., 2015).

The Akt family includes three members: (1) *Akt1* is involved in cellular survival pathways (Chen et al., 2001), and gene levels were elevated in muscle of *Cpt1b*^{m^{-/-}} mice; (2) *Akt2* is an important molecule in the insulin signaling pathway (Garofalo et al., 2003), but mRNA expression was not different between genotypes; and (3) *Akt3* was undetectable in skeletal muscle (Figure 2D). Phosphorylation of Akt1 (Ser473) at baseline was not different between genotypes, but insulin-stimulated phosphorylation was significantly greater in skeletal muscle of *Cpt1b*^{m^{-/-}} mice (Figure 2E). Phosphorylation of Akt2 (Ser474) at baseline was significantly decreased in muscle of *Cpt1b*^{m^{-/-}} mice compared to *Cpt1b*^{fl/fl} mice, whereas insulin-stimulated Akt2 phosphorylation was comparable between genotypes (Figure 2F).

To gain further insight into how impaired mitochondrial FAO causes inhibition of mTORC1 signaling, we next examined upstream factors that affect the mTORC1 pathway. TSC1/TSC2 is a critical regulator of mTOR signaling, and activation of this complex inhibits mTORC1 (Wullschleger et al., 2006). In contrast, TSC1/TSC2 activates mTORC2, which in turn triggers Akt1 activation (Huang and Manning, 2009). Within the TSC1/TSC2 complex, TSC1 stabilizes TSC2 (Chong-Kopera et al., 2006), which facilitates activation of TSC2 by kinases such as AMPK and Akt that directly phosphorylate TSC2 at Ser1387 (Inoki et al., 2003) and Thr1462 (Huang and Manning, 2008), respectively. We found significantly elevated phosphorylation of TSC2 at Ser1387 in muscle of *Cpt1b*^{m^{-/-}} mice, whereas phosphorylation of TSC2 at Thr1462 was not different. These findings suggest TSC2 activation occurs via AMPK but not Akt in *Cpt1b*^{m^{-/-}} muscle (Figure 2G). This is consistent with our previous report that mitochondrial FAO deficiency induced a low-energy state in skeletal muscle of *Cpt1b*^{m^{-/-}} mice that activated AMPK (Wicks et al., 2015) but extends these findings by suggesting that AMPK stimulates the TSC1/TSC2 complex in *Cpt1b*^{m^{-/-}} mice (Figure 2H). Specifically, these findings suggest that TSC1/TSC2 inhibits mTORC1 signaling, resulting in enhanced basal insulin sensitivity, and activates the mTORC2 pathway in *Cpt1b*^{m^{-/-}} mice, which increases basal glucose uptake (Figure 2H).

Fgf21 Induction in *Cpt1b*-Deficient Muscle Is AMPK and Akt1 Dependent

Within the model shown in Figure 2H, we predict AMPK and Akt1 signaling are necessary for induction of FGF21 in skeletal muscle of *Cpt1b*^{m^{-/-}} mice. To test this directly, we used mouse and human primary muscle cells. In agreement with our mechanistic hypothesis (Figure 2H), expression of *Fgf21* in primary myotubes from *Cpt1b*^{m^{-/-}} mice was normalized when exposed to either an Akt1-specific inhibitor, A-674563, or an AMPK inhibitor, compound C (Figure 3A). To test whether pharmacological inhibition of CPT1b recapitulates effects of genetic inhibition of *Cpt1b*, we exposed primary myotubes from *Cpt1b*^{fl/fl} mice to fatty acid (FA) in the presence of the CPT1 inhibitor, etomoxir. *Fgf21* expression was not induced in the presence of FA alone but was robustly elevated in myotubes exposed to FA in the presence of etomoxir in a dose-dependent manner (Figures 3B and S2C).

To study whether the pharmacological inhibition of CPT1 drives FGF21 induction in the insulin-resistant condition, we

explored human skeletal muscle myotubes from diabetic-obese subjects. Our previous report demonstrated that these myotubes are insulin-resistant compared to myotubes derived from non-diabetic-lean (normal-lean) humans (Vandanmagsar et al., 2014). Treatment with FA induced FGF21 expression in the presence of etomoxir in myotubes from both normal-lean and diabetic-obese subjects; however, FGF21 induction was blunted in myotubes from diabetic-obese subjects (Figure 3C). Exposure to A-674563 and compound C blunted FA + etomoxir induction of FGF21 in myotubes from both groups (Ferré, 2004). FGF21 is induced by PPAR α in liver in response to fasting (Inagaki et al., 2007). However, treatment with inhibitors of PPAR α , PPAR γ , and PPAR δ did not affect FA + etomoxir-induced FGF21 expression in myotubes from normal-lean subjects (Figure 3D). Collectively, these data indicate involvement of AMPK and Akt1 signaling in FGF21 induction in the mitochondrial FAO-deficient condition.

To test whether FGF21 directly imparts beneficial effects on the insulin signaling cascade in the presence of excess FA, we treated human myotubes from normal-lean subjects with rhFGF21 \pm FA and determined activity of mTOR and its downstream signaling pathways. In the absence of FA, FGF21 had minimal effects, because only phosphorylation of p70S6K was reduced. Alternatively, when FA was present, FGF21 was able to reduce phosphorylation of mTOR (Ser2448), p70S6K, IRS1 (Ser636/639), and Akt (Ser473) (Figure 3E). Taken together, these data suggest that FGF21 has protective effects on lipid-induced insulin resistance, which in turn preserves glucose uptake in muscle in lipotoxic conditions, such as in skeletal muscle of *Cpt1b*^{m^{-/-}} mice.

Stress Signaling Pathways Are Not Activated by Mitochondrial Fat Oxidation Deficiency

To determine whether other potential signaling pathways lead to induction of FGF21 in skeletal muscle of *Cpt1b*^{m^{-/-}} mice, we evaluated other mechanisms linked to mTOR signaling and FGF21 induction. In *Cpt1b*^{m^{-/-}} mice, systemic and intramyocellular lipids, particularly toxic diacylglycerol (DAG) species, are increased (Wicks et al., 2015); thus, DAG signaling could be enhanced. Previous reports have shown that DAG kinases inhibit mTOR activation by repressing Erk1/2 pathways (Gorentla et al., 2011). Erk1/2 directly phosphorylates TSC2, thus negatively regulating mTORC1 signaling (Ma et al., 2005; Wullschleger et al., 2006). Phosphorylation of Erk1/2 was not elevated in skeletal muscle of *Cpt1b*^{m^{-/-}} mice (Figure 4A). In addition, oxidative stress and hypoxia have been linked to mTORC1 activity (Kim et al., 2002; Wouters and Koritzinsky, 2008). Gene expression of oxidative stress (*Nrf2*) and hypoxia (*Hif1 α*) markers was not elevated in muscle of *Cpt1b*^{m^{-/-}} mice compared to *Cpt1b*^{fl/fl} mice (Figures 4B and 4C). Furthermore, the expression levels of ER stress markers (unspliced *Xbp1u* and spliced *Xbp1s*) were unchanged in *Cpt1b*^{m^{-/-}} muscle (Figure 4D). Moreover, ER stress marker *Ddit3* (Haynes and Ron, 2010) expression was significantly decreased in *Cpt1b*^{m^{-/-}} muscle (Figure 4E). In line with these data, *Atf4* mRNA and protein expression and *Atf5* mRNA expression in skeletal muscle were similar between *Cpt1b*^{m^{-/-}} and *Cpt1b*^{fl/fl} mice (Figures 4F and S2D).

In addition to the candidate gene approach, we did a comprehensive global expression analysis in gastrocnemius muscle

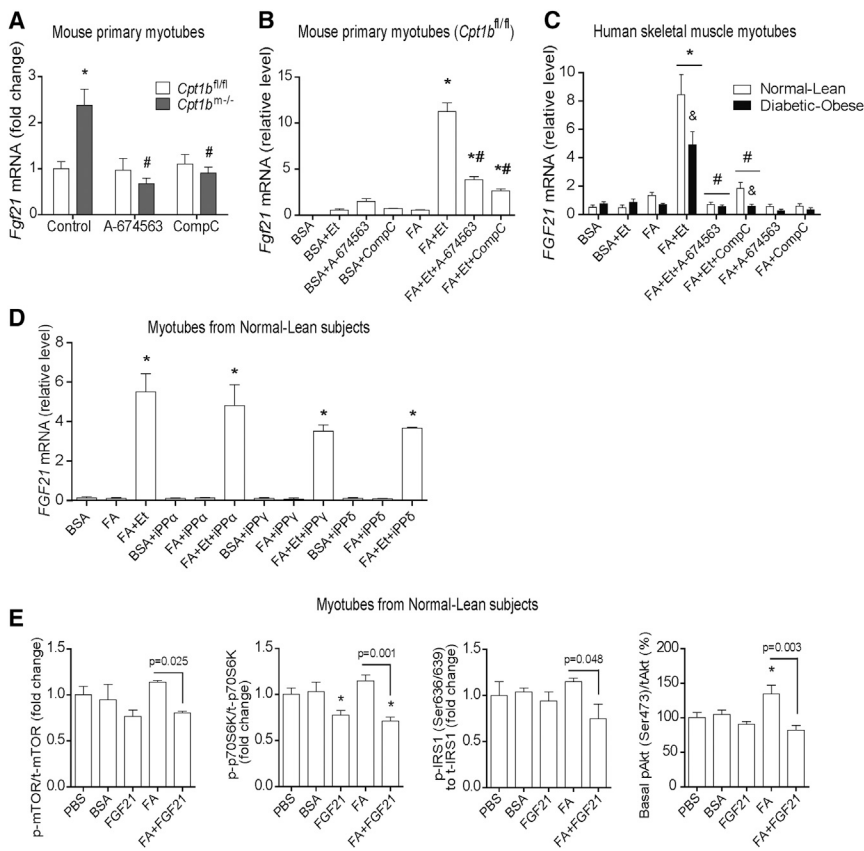


Figure 3. Fgf21 Induction in Skeletal Muscle of *Cpt1b*^{−/−} Mice Is AMPK and Akt1 Dependent

(A and B) Gene expression of *Fgf21* in mouse primary myotubes treated with an Akt1 inhibitor, A-674563 (30 μM), and an AMPK inhibitor, compound C (CompC, 30 μM), for 24 hr. (A) Results shown are representative of three independent cultures. **p* < 0.05 between *Cpt1b*^{−/−} and *Cpt1b*^{fl/fl} mice, and #*p* < 0.05 between treatments with vehicle and inhibitors. (B) Primary muscle cells from *Cpt1b*^{fl/fl} mice. Myotubes were treated with BSA-conjugated FA (FA, 0.5 mM) in the presence of the Cpt1 inhibitor etomoxir (Et, 100 μM) for 24 hr. Results shown are representative of three or four separate experiments. **p* < 0.05 between control (BSA) and other treatments, and #*p* < 0.05 due to Akt1 or AMPK inhibitors.

(C) Gene expression of *FGF21* in human myotubes treated with FA (0.5 mM) and inhibitors Et (100 μM), A-674563 (50 μM), and CompC (30 μM) for 24 hr. HSMMs derived from normal-lean and diabetic-obese subjects were differentiated into myotubes before treatments (n = 4 per group). Results shown are representative of two independent cultures of HSMM per subject. **p* < 0.05 between treatments with FA and inhibitors, #*p* < 0.05 due to Akt1 or AMPK inhibitors, and &*p* < 0.05 between myotubes from normal-lean and diabetic-obese subjects.

(D) Gene expression of *FGF21* in human myotubes treated with FA (0.5 mM) and Et (100 μM) and PPAR inhibitors GW6471 (for PPARα, 10 μM), T0070907 (for PPARγ, 10 μM), and GSK3787 (for PPARδ, 10 μM) for 24 hr. **p* < 0.05 between treatments with inhibitors and BSA control.

(E) Activity of mTORC1 and its downstream signaling members P70S6K, IRS1, and basal Akt, as determined by phosphorylation in human myotubes. HSMMs originating from normal-lean subjects were differentiated into myotubes before treatment with FA (0.5 mM) and rhFGF21 (200 ng/ml). **p* < 0.05 between vehicle (PBS) and other treatments.

All data are presented as mean ± SEM.

from *Cpt1b*^{−/−} and control mice. The genes belonging to ER stress, autophagy, and mitophagy pathways were obtained from gene ontology and then compared by pathway enrichment analysis by including these three pathways to the standard Kyoto Encyclopedia of Genes and Genomes (KEGG) pathways. None of these overall pathways were significantly different between *Cpt1b*^{−/−} and *Cpt1b*^{fl/fl} mice (Figure 4G). At the gene level, only 1 gene (*Ppp1r15a*) out of more than 200 genes was significantly different between *Cpt1b*^{−/−} and control mice. Heatmaps showing the distribution of expression for genes belonging to these pathways are included in Supplemental Information (Figures S3–S5). Moreover, uncoupling protein 3 (*Ucp3*) expression was significantly increased in *Cpt1b*^{−/−} muscle (Figure 4H), suggesting potential beneficial effects, because it has been reported that upregulated expression of UCP3 reduced ER stress (Xu et al., 2015) and reactive oxygen species (ROS) production (Nabben et al., 2011). Together, these data indicate that mitochondrial respiratory chain dysfunction and myocellular stress do not appear to be major inducers of FGF21 in *Cpt1b*^{−/−} muscle and are consistent with our previous report that *Cpt1b*-deficient mitochondria respire efficiently when given substrates other than long-chain fatty acids (Wicks et al., 2015). Pathways for oxidative phosphorylation, tricarboxylic acid (TCA) cycle,

and overall mitochondrial biogenesis are upregulated in *Cpt1b*^{−/−} muscle (Wicks et al., 2015).

Loss of FGF21 Increases Muscle Mass, Activity, Energy Expenditure, and Oxidative Capacity but Does Not Alter Adiposity in *Cpt1b*^{−/−} Mice

To determine the extent of FGF21's role in the overall phenotype of *Cpt1b*^{−/−} mice, we generated DKO mice (*Fgf21*^{−/−}*Cpt1b*^{−/−}) by crossing *Fgf21*^{−/−} mice (Badman et al., 2009; Hotta et al., 2009) with *Cpt1b*^{−/−} mice. As shown in Figure 5A, there was an intermediate effect on body weight in DKO mice. DKO mice were significantly heavier than *Cpt1b*^{−/−} mice but did not reach the body weight of control or *Fgf21*^{−/−} mice (Figure 5A). However, there was no difference in fat mass between *Cpt1b*^{−/−} and DKO mice, as measured by nuclear magnetic resonance (NMR) (Figure 5B) or by the weight from individual fat pads (Figure 5D). Fat-free mass (FFM) was significantly increased in DKO compared to *Cpt1b*^{−/−} mice (Figure 5C). Gastrocnemius and quadriceps muscles were heavier in both DKO and *Fgf21*^{−/−} mice, but liver, kidney, and heart weights were not significantly higher in DKO compared to *Cpt1b*^{−/−} mice (Figure 5D). Body length was significantly decreased in both *Cpt1b*^{−/−} and DKO mice compared to control mice, whereas *Fgf21*^{−/−} mice appeared

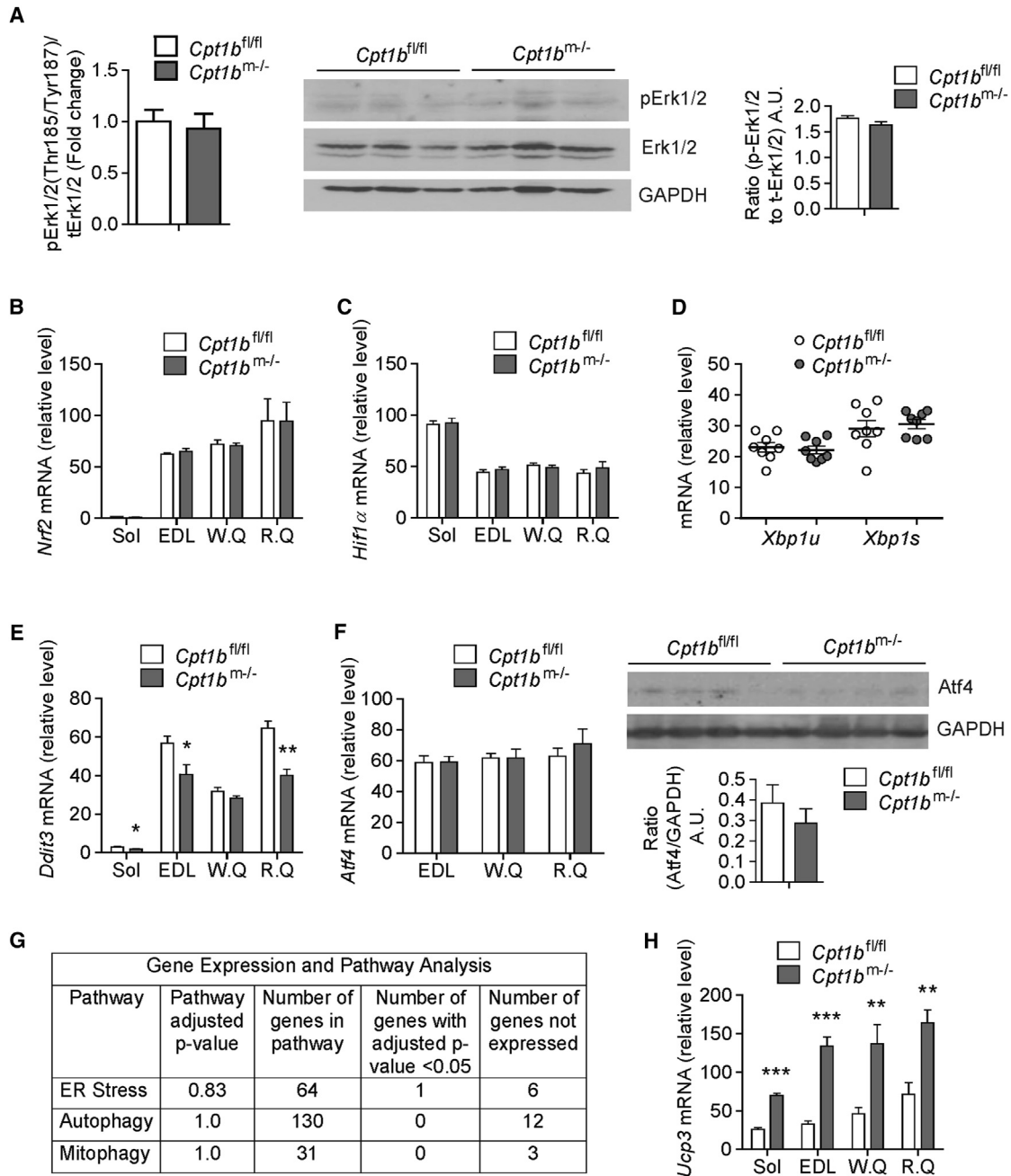


Figure 4. Stress Signaling Pathways that Are Not Activated by Mitochondrial Fat Oxidation Deficiency

(A) Activity of Erk1/2 signaling pathway, as determined by multiplex protein signaling assay (left) and western blot analysis (center) for phosphorylation in gastrocnemius muscle from 4-month-old *Cpt1b^{m-/m-}* and *Cpt1b^{fl/fl}* mice (n = 3–4 per group). The Thr185/Tyr187 antibody detects phosphorylation at Thr185 and Tyr187. GAPDH was used as a loading control. ImageJ software was used for densitometry quantification of the immunoblots (right).

(B and C) Gene expression of oxidative stress (B) and hypoxia (C) markers, as examined by qRT-PCR in muscle.

(D and E) ER stress markers in muscle. Gene expression of unspliced and spliced *Xbp1* (D) and *Ddit3* (E), as determined by qRT-PCR in muscle tissue

(F) Gene and protein expression of Atf4, as detected by qRT-PCR and western blot, respectively, in skeletal muscle.

(G) Summary of results from gene expression and pathway analysis for ER stress, autophagy, and mitophagy using gene ontology and pathway enrichment analysis on SAGE (serial analysis of gene expression) data obtained from gastrocnemius muscle.

(H) Gene expression of uncoupled protein 3 (*Ucp3*), as evaluated by qRT-PCR in skeletal muscle. Gene expression analysis was performed in muscle tissue such as soleus (Sol), extensor digitorum longus (EDL), white and red quads (W.Q. and R.Q.), and gastrocnemius from 4-month-old *Cpt1b^{m-/m-}* and *Cpt1b^{fl/fl}* mice (n = 6–8 per group). Immunoblot analysis was performed in gastrocnemius muscle from 4-month-old *Cpt1b^{m-/m-}* and *Cpt1b^{fl/fl}* mice. Results shown are representative of three independent experiments (n = 4–6 per group).

All data are presented as mean ± SEM. *p < 0.05, **p < 0.01, and ***p < 0.005 and higher significance.

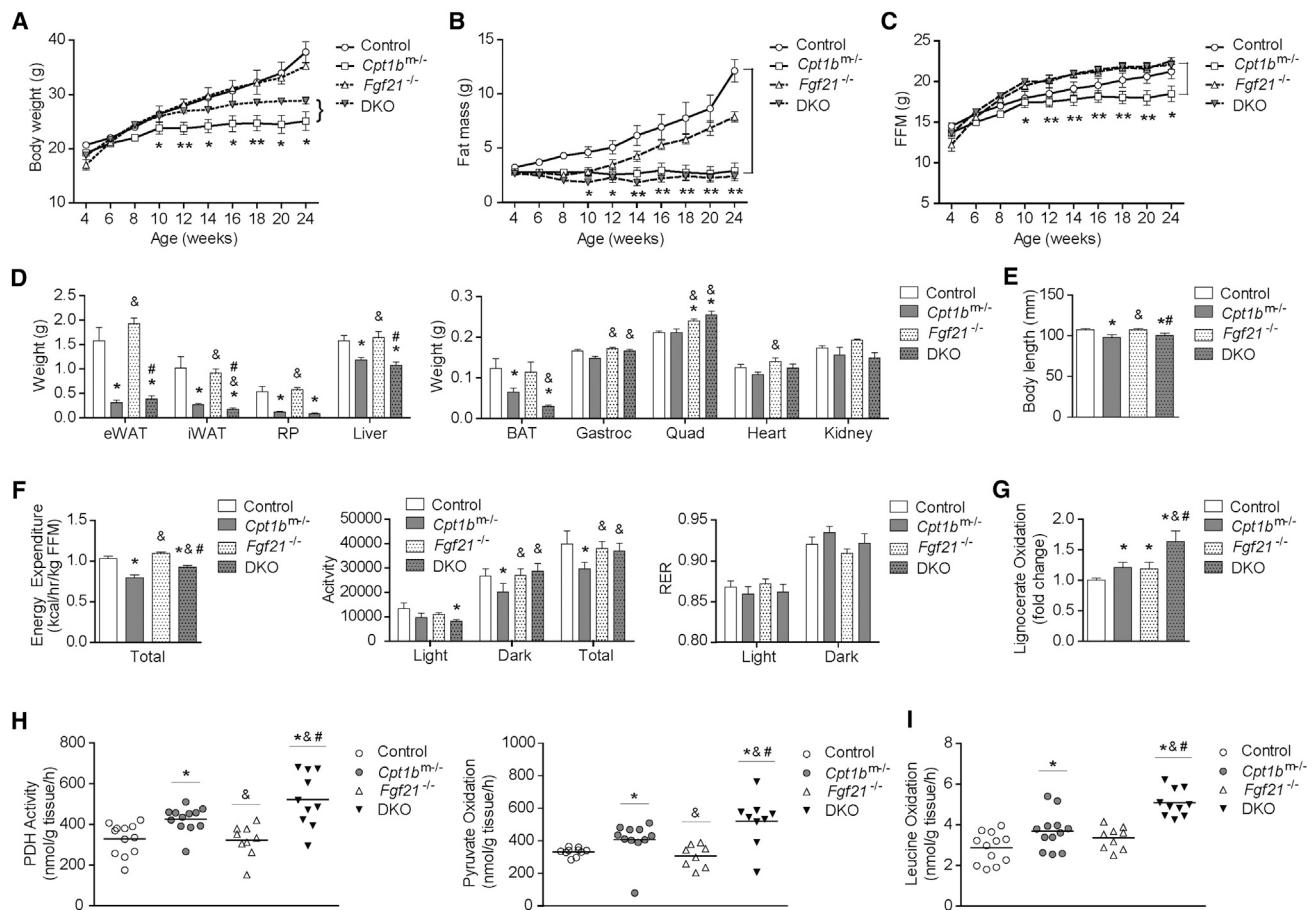


Figure 5. Loss of FGF21 Increases Muscle Mass, Activity, Energy Expenditure, and Oxidative Capacity but Does Not Alter Adiposity in *Cpt1b^{m/-}* Mice

(A–C) Body weight (A), fat mass (B), and FFM (C) (n = 7 per group).

(D) Tissue weights (n = 7).

(E) Body length (n = 8–14).

(F) Energy expenditure, activity level, and RER (n = 4–6 per group).

(G–I) Substrate oxidation measured in gastrocnemius muscle homogenate from control [*Fgf21^{+/+}Cpt1b^{fl/fl}*], *Cpt1b^{m/-}* [*Fgf21^{+/+}Cpt1b^{m/-}*], *Fgf21^{-/-}* [*Fgf21^{-/-}Cpt1b^{fl/fl}*], and DKO [*Fgf21^{-/-}Cpt1b^{m/-}*] mice: (G) peroxisomal FAO measured from [¹⁻¹⁴C]lignoceric acid (20 μM), (H) PDH activity assayed with [¹⁻¹⁴C]pyruvate and pyruvate oxidation measured with [³⁻¹⁴C]pyruvate, and (I) leucine oxidation measured from [¹⁻¹⁴C]leucine (100 μM) (n = 8–12 per group).

All data are presented as mean ± SEM. (A–C) *p < 0.05 significance when *Cpt1b^{m/-}* mice were compared to control and DKO mice. (D–I) *p < 0.05 significance compared to control mice, #p < 0.05 significance compared to *Fgf21^{-/-}* mice, and &p < 0.05 significance compared to *Cpt1b^{m/-}* mice.

to have body length significantly longer than that of *Cpt1b^{m/-}* and DKO mice (Figure 5E). *Cpt1b^{m/-}* mice have reduced activity, leading to an overall decrease in energy expenditure (Figure 5F) (Wicks et al., 2015). The decreased activity in *Cpt1b^{m/-}* mice is almost restored by the lack of FGF21 in DKO mice with a concomitant increase in energy expenditure (Figure 5F). In addition, the respiratory exchange ratio (RER) in DKO mice was comparable to that in control mice (Figure 5F).

As we previously reported, inhibition of mitochondrial FAO specifically in skeletal muscle results in favorable metabolic adaptations in muscle, such as compensatory increases in carbohydrate oxidation, amino acid oxidation, and peroxisomal fat oxidation (Wicks et al., 2015). Likewise, we observed increased peroxisomal oxidation of the very long-chain fatty acid lignocer-

ate (Figure 5G), enhanced pyruvate dehydrogenase (PDH) activity and pyruvate oxidation through the TCA cycle (Figure 5H), and leucine oxidation in skeletal muscle homogenates from *Cpt1b^{m/-}* mice compared to those from control mice (Figure 5I). The expression of mitochondrial biogenesis genes in muscle of DKO was comparable to the increased level in *Cpt1b^{m/-}* muscle (Figure S6A). Loss of FGF21 had little effect on oxidation, but the combined loss of CPT1b and FGF21 in DKO mice further increased PDH activity and increased pyruvate oxidation through the TCA cycle, leucine oxidation, and peroxisomal oxidation (Figures 5G–5I). In summary, overall fat mass is not increased in DKO mice. Rather, elevated FGF21 in *Cpt1b^{m/-}* mice seems to negatively regulate muscle mass, activity, and energy expenditure.

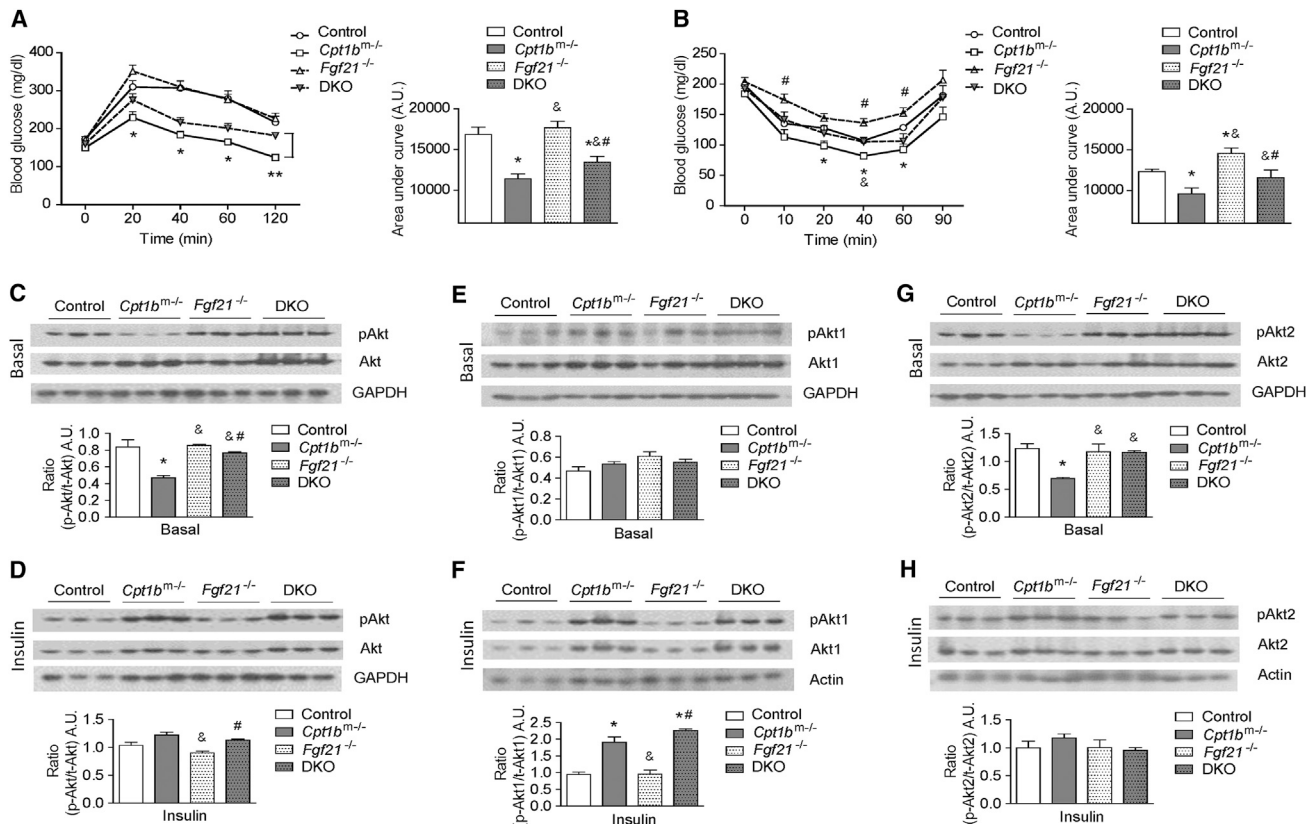


Figure 6. FGF21 Is Responsible for Increased Glucose Utilization in *Cpt1b*^{m-/-} Muscle

(A and B) GTT (A; n = 14–22 per group) and ITT (B; n = 7–11 per group).

(C–H) Immunoblot analysis of Akt proteins. Basal (C) and insulin-stimulated (D) phosphorylation of total Akt at Ser473. Basal (E) and insulin-stimulated (F) phosphorylation of Akt1 at Ser473. Basal (G) and insulin-stimulated (H) phosphorylation of Akt2 at Ser474. GAPDH was used as a loading control. Results shown are representative of three independent experiments. Gastrocnemius muscle from control (*Fgf21*^{+/+} *Cpt1b*^{fl/fl}), *Cpt1b*^{m-/-} (*Fgf21*^{+/+} *Cpt1b*^{m-/-}), *Fgf21*^{-/-} (*Fgf21*^{-/-} *Cpt1b*^{fl/fl}), and DKO (*Fgf21*^{-/-} *Cpt1b*^{m-/-}) mice were used for all immunoblot analyses (n = 3–5 per group). ImageJ software was used for densitometry quantification of the immunoblots.

All data are presented as mean ± SEM. (A and B) *p < 0.05 significance between control and *Cpt1b*^{m-/-} mice, #p < 0.05 significance between *Cpt1b*^{m-/-} and *Fgf21*^{-/-} mice, and &p < 0.05 significance between *Cpt1b*^{m-/-} and DKO mice. (C–H) *p < 0.05 significance compared to control mice, #p < 0.05 significance compared to *Fgf21*^{-/-} mice, and &p < 0.05 significance compared to *Cpt1b*^{m-/-} mice.

Glucose Utilization and Insulin Signaling Are Partially Regulated by FGF21 in *Cpt1b*^{m-/-} Mice

Blood glucose levels are significantly decreased in *Cpt1b*^{m-/-} mice compared to control (*Cpt1b*^{fl/fl}) mice during a glucose tolerance test (GTT), indicating improved glucose clearance. This improvement was partially negated in DKO mice compared to *Cpt1b*^{m-/-} mice (Figure 6A). Compared to control mice, insulin-stimulated glucose clearance was also improved in *Cpt1b*^{m-/-} mice during an insulin tolerance test (ITT). Similar to the GTT, these improvements in insulin sensitivity were negated in DKO mice compared to *Cpt1b*^{m-/-} mice (Figure 6B). Consistent with this, basal phosphorylation of Akt (Ser473) in skeletal muscle of DKO mice was significantly higher compared to *Cpt1b*^{m-/-} muscle, whereas it was significantly lower compared to *Fgf21*^{-/-} muscle and was indifferent compared to control mice muscle (Figure 6C). However, insulin-stimulated phosphorylation of Akt (Ser473) in muscle of DKO was comparable to levels in control and *Cpt1b*^{m-/-} muscle (Figure 6D). Phosphorylation of Akt1 (Ser473) at baseline was not different among all ge-

notypes (Figure 6E). However, Akt1 phosphorylation in response to insulin in muscle of DKO mice was similar to *Cpt1b*^{m-/-} muscle and was significantly increased compared to control mice muscle (Figure 6F), indicating again that *Fgf21* is downstream of Akt1 signaling in *Cpt1b*-deficient muscle (Figure 2H). Reduced phosphorylation of Akt2 (Ser474) at baseline in skeletal muscle of *Cpt1b*^{m-/-} mice was reversed in muscle from DKO mice so that it was comparable to that from control mice (Figure 6G), whereas Akt2 phosphorylation in response to insulin was comparable among all genotypes (Figure 6H). These data reinforce a possible feedback inhibition of mTORC1 by FGF21, through which FGF21 contributes to enhanced basal insulin sensitivity in *Cpt1b*^{m-/-} mice (Figure 2H).

Muscle-Derived FGF21 Promotes Browning of Inguinal WAT in *Cpt1b*^{m-/-} Mice

Because serum FGF21 levels were significantly higher in both fed and fasted states in *Cpt1b*^{m-/-} mice (Figure 1A), we examined FGF21 signaling in other metabolic tissues in *Cpt1b*^{m-/-}

mice. Gene expression of *Klb* and *Fgfr1b* was significantly increased in WAT of *Cpt1b^{m-/-}* mice compared to *Cpt1b^{fl/fl}* mice without changes in *Fgfr1c* expression, which would facilitate enhanced FGF21 signaling in WAT (Figures 7A, 7B, and S6B). Consistent with previous reports that FGF21 exerts metabolic action enhancing lipolysis, fat oxidation (Coskun et al., 2008), and accumulation of beige adipocytes in other metabolic tissues (Fisher et al., 2012; Keipert et al., 2014), expression of *Pnpla2*, *Hadha*, and *Cs* genes was significantly upregulated in WAT of *Cpt1b^{m-/-}* mice compared to control mice, without affecting liver expression (Figures 7C–7E and S6C). Collectively, these data are consistent with elevated lipolysis and lipid oxidation in WAT depots but not in liver of *Cpt1b^{m-/-}* mice (Figures 7C–7E and S6C). This seems to be at least partially mediated via FGF21, because DKO mice exhibit significantly attenuated gene expression of the lipolytic marker *Pnpla2* (*Atgl*) in WAT of DKO mice compared to *Cpt1b^{m-/-}* mice (Figure 7C), as well as reduced expression of fat oxidation markers *Hadha* and *Cs* in inguinal WAT (iWAT) of DKO mice (Figures 7D and 7E). Alternatively, *Hadha* and *Cs* gene expression was similar in epididymal WAT (eWAT) of DKO mice compared to *Cpt1b^{m-/-}* mice (Figures 7D and 7E).

In addition, expression of brown adipocyte markers such as *Ucp1* and *Cidea* was significantly increased in iWAT, but not in eWAT, of *Cpt1b^{m-/-}* mice compared to control mice (Figures 7F and S6D). Expression of *Ucp1* and *Cidea* was entirely attenuated in iWAT of *Fgf21^{-/-}* and DKO mice compared to *Cpt1b^{m-/-}* mice (Figure 7F). Given the reversal of FAO enzymes and *Ucp1* and *Cidea* expression by loss of FGF21 in DKO mice, increased fat mass might be expected. However, neither fat mass by NMR (Figure 5B) nor individual fat pad weight (Figure 5D) were different between DKO mice and *Cpt1b^{m-/-}* mice. In addition, there is an obvious decrease in adipocyte size in *Cpt1b^{m-/-}* mice compared to control mice that is not changed by the loss of FGF21 (Figure 7G).

Effects on Liver, Pancreas, IGF-1, and Adiponectin in *Cpt1b^{m-/-}* Mice

The pancreas and liver are both known producers and targets of FGF21 (Fon Tacer et al., 2010). In Figure 1B, we reported no increase in FGF21 expression in liver of *Cpt1b^{m-/-}* mice. Likewise, the expression of *Klb*, *Fgfr4*, and *Fgfr1c* in liver of *Cpt1b^{m-/-}* mice was unaltered compared to *Cpt1b^{fl/fl}* mice (Figures S6E and S6F). Expression of *Fgfr1b* was significantly increased in liver of *Cpt1b^{m-/-}* mice. However, the expression level was negligible compared to expression of other Fgf receptors in liver (Figure S6F). In addition, gene expression of *Fgf21* and of *Klb* and *Fgf* receptors in pancreas was comparable between *Cpt1b^{m-/-}* and *Cpt1b^{fl/fl}* mice (Figures S6G and S6H).

In a transgenic animal model, it has been shown that FGF21-overexpressing mice have significantly lower levels of IGF-1 compared to wild-type mice (Inagaki et al., 2008). Serum levels of IGF-1 were significantly lower in *Cpt1b^{m-/-}* mice ($n = 52–59$) (Figure S7A). In a smaller cohort, IGF-1 was significantly lower in *Cpt1b^{m-/-}* mice and DKO mice compared to control and *Fgf21^{-/-}* mice (Figure S7B). These data are consistent with decreased body length in *Cpt1b^{m-/-}* and DKO mice (Figure 5E), but they do not suggest that reduced IGF-1 is driven by

increased circulating FGF21 in *Cpt1b^{m-/-}* mice. Though the metabolic effect of FGF21 has been shown to be dependent upon adiponectin (Holland et al., 2013), the expression of adiponectin receptors, *Adipor1* and *Adipor2*, was not different in skeletal muscle between *Cpt1b^{m-/-}* and *Cpt1b^{fl/fl}* mice (Figures S6C and S6D). Serum levels of total and high molecular weight adiponectin were also similar between *Cpt1b^{m-/-}* and *Cpt1b^{fl/fl}* mice (Figures S6E and S6F). This is consistent with a paper (Kolumam et al., 2015) demonstrating FGF21 mimetic antibody has metabolic effects in adiponectin-knockout mice.

DISCUSSION

Previously, we showed that AMPK/PGC1 α activated by energy deprivation orchestrates compensatory increases in mitochondrial biogenesis, mitochondrial oxidative capacity, fat oxidation by peroxisomes, and usage of amino acids as energy sources in *Cpt1b^{m-/-}* muscle (Wicks et al., 2015). Here we show that AMPK, through activation of the TSC complex, (1) activates mTORC2-Akt1-FGF21, leading to an increase in Glut1, and (2) inactivates mTORC1-S6K-IRS-1 serine phosphorylation. Both stimulate glucose uptake at low insulin levels.

The induction of FGF21 in response to impaired mitochondrial FAO in skeletal muscle is a part of several compensatory adaptations designed to maintain energy supply to muscle in *Cpt1b^{m-/-}* mice. While liver is considered the major organ for the upregulation and secretion of FGF21 in an energy- or nutrient-deficient state, muscle has also been shown to secrete FGF21. Energy deficit caused by respiratory chain deficiencies leads to mitochondrial myopathy and increased FGF21 production in mice and humans (Suomalainen et al., 2011; Tyynismaa et al., 2010). In another model of mitochondrial inefficiency, muscle-specific overexpression of UCP-1 causes FGF21 upregulation in skeletal muscle (Keipert et al., 2014; Ost et al., 2015). Dysregulation of lipid delivery to mitochondria by either overexpression of perilipin 5 (Harris et al., 2015) or deletion of the lipase ATGL (Brahma et al., 2014), leads to FGF21 induction in skeletal muscle or heart, respectively. Taken together with our data, these results suggest that many pathophysiological conditions (disorders of lipid uptake and transport, lipid droplet formation and lipolysis, any defect in the carnitine shuttle system, disorders of mitochondrial FAO, and mitochondrial dysfunction) stimulate FGF21 production in muscle.

All preceding models represent rather severe conditions that identified specific pathways for FGF21 regulation in muscle. While still not physiological, one study demonstrated that after a prolonged 3–4 hr hyperinsulinemic-euglycemic clamp, both skeletal muscle FGF21 mRNA and circulating FGF21 were increased (Hojman et al., 2009). The hyperinsulinemic-euglycemic clamp procedure can be considered a period of suppression of FAO. In the present study, we demonstrate that there is minimal FGF21 expression in murine or human primary myotubes and that incubation of either murine or human primary myotubes with a palmitate-oleate mixture or the CPT1 inhibitor etomoxir alone has no effect on FGF21 mRNA. However, the combination of fatty acids and etomoxir increases FGF21 expression nearly 10-fold (Figures 3A–3C). We also demonstrate that FGF21 induction is blunted in differentiated myotubes from obese-diabetic

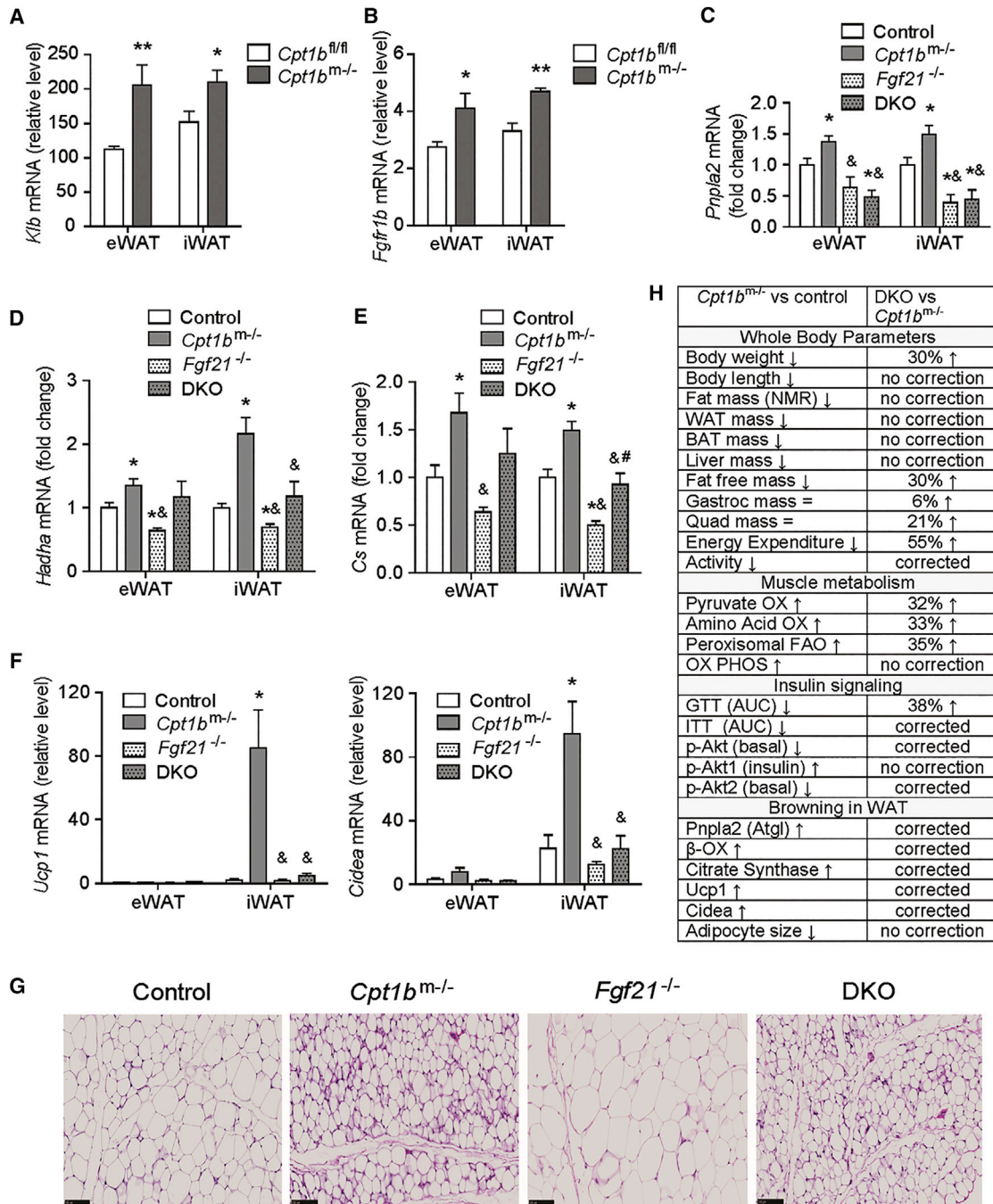


Figure 7. Muscle-Derived FGF21 Enhances Browning in WAT in *Cpt1b^{m/-}* Mice

(A and B) Gene expression of *Klb* (A) and *Fgfr1b* (B) in eWAT and iWAT (n = 5–7 per group).

(C–F) qRT-PCR analysis of expression of a lipolytic gene (*Pnpla2*; C), mitochondrial FAO genes (*Hadha* and *Cs*; D and E), and beige adipocyte marker genes (*Ucp1* and *Cidea*; F) in WAT.

(G) H&E staining of iWAT. Scale bar represents 100 μ m.

(H) Summary of the phenotype in *Cpt1b^{m/-}* mice compared to control mice and the reverse phenotype in DKO mice. Tissue from control (*Fgf21^{+/+} Cpt1b^{fl/fl}*), *Cpt1b^{m/-}* (*Fgf21^{+/+} Cpt1b^{m/-}*), *Fgf21^{-/-}* (*Fgf21^{-/-} Cpt1b^{fl/fl}*), and DKO (*Fgf21^{-/-} Cpt1b^{m/-}*) mice was used for all qRT-PCR analysis (n = 5–7 per group).

All data are presented as mean \pm SEM. (A and B) *p < 0.05 and **p < 0.005 and higher significance. (C–F) *p < 0.05 significance compared to control mice, #p < 0.05 significance compared to *Fgf21^{-/-}* mice, and &p < 0.05 significance compared to *Cpt1b^{m/-}* mice.

subjects. Moreover, we observe decreased mitochondrial FAO induces FGF21 in otherwise “healthy” myotubes. We also demonstrate that the regulation of FGF21 production appears to be mediated through an AMPK-mTOR-Akt1 axis (Figures 3A–3C). This is in agreement with a transgenic mouse model, in which overexpression of Akt1 induces FGF21 secretion from muscle (Izumiya et al., 2008). Two previous studies report beneficial effects of FGF21 treatment on human myotubes by increasing glucose uptake (Mashili et al., 2011) and suppressing necrosis factor κ B (Lee et al., 2012). We further show that FGF21 has beneficial effects in human myotubes. FGF21 was able to repress mTORC1, leading to subsequent repression of IRS1 phosphorylation at Ser636/639 and improved downstream insulin signaling in the presence of FA.

Numerous studies demonstrate that the induction of FGF21 requires an ATF4-dependent mechanism (De Sousa-Coelho et al., 2012; Kim et al., 2013a; Kim et al., 2013b; Ost et al., 2015; Tynnismaa et al., 2010). We were surprised to see no changes in *Atf4* mRNA or protein levels in *Cpt1b*^{m−/−} mice. In addition, markers for oxidative stress (*Nrf2*), hypoxia (*Hif1 α*), and ER stress (unspliced *Xbp1u* and spliced *Xbp1s*, *Ddit3*) were not elevated in *Cpt1b*^{m−/−} muscle (Figure 4). In addition, a comprehensive global expression analysis demonstrated that ER stress, autophagy, and mitophagy pathways are not significantly different between *Cpt1b*^{m−/−} and control mice (Figures S3–S5). Despite the accumulation of total lipid and lipotoxic intermediates, the skeletal muscle from *Cpt1b*^{m−/−} mice has characteristics similar to that from trained athletes (Goodpaster et al., 2001), including increased glucose and lipid uptake, large lipid droplets, increased mitochondrial biogenesis, and increased mitochondrial oxidative capacity, although *Cpt1b*^{m−/−} mice are hypoactive (Wicks et al., 2015).

When we investigated the role of muscle-derived FGF21 in the obesity-resistant phenotype in *Cpt1b*^{m−/−} mice at the whole-body level (see Figure 7H for summary), DKO mice showed a modest attenuation in the body weight reduction observed in *Cpt1b*^{m−/−} mice. However, the increase in body weight between *Cpt1b*^{m−/−} and DKO mice was entirely accounted for by an increase in FFM in DKO mice. The decreased fat mass and body length observed in *Cpt1b*^{m−/−} mice was not corrected by the absence of FGF21. Examination of individual tissues again shows that the reduced fat mass in *Cpt1b*^{m−/−} mice is not increased in DKO mice. Likewise, the mass of major organs, such as liver, heart, and kidney, is still reduced in DKO mice. We did observe an increase in skeletal muscle mass in both *Fgf21*^{−/−} and DKO mice, which is probably responsible for the increased FFM. The reduced spontaneous activity observed in *Cpt1b*^{m−/−} mice is normalized in DKO mice. The increased activity may be supported by the increased muscle mass rather than the known effects of FGF21 on torpor and circadian rhythms (Bookout et al., 2013), because activity in *Fgf21*^{−/−} mice is not greater than that in control mice (Figure 5).

The improved glucose uptake during a GTT was partially blunted in DKO mice, and the marginal decrease in blood glucose during an ITT was returned to control levels in DKO mice. At the muscle level, the reduced phosphorylation of Akt2 at baseline in *Cpt1b*^{m−/−} muscle was substantially reversed in muscle of DKO mice, indicating that FGF21 contributes largely

to the improvement in basal insulin sensitivity in *Cpt1b*^{m−/−} muscle. When we investigated the role of FGF21 in the increased oxidative capacity of *Cpt1b*^{m−/−} muscle, we found that DKO mice showed further increases in peroxisomal fat, carbohydrate, and amino acid oxidation. A potential explanation is that beneficial effects of FGF21 on glucose uptake are gone in DKO mice and that the muscle is further compensating to increase oxidative capacity.

FGF21 has been reported to ameliorate diet-induced obesity and insulin resistance by increasing lipolysis and β -oxidation (Coskun et al., 2008; Inagaki et al., 2007; Kharitononkov et al., 2005). We detected elevated markers of mitochondrial number, lipolysis, β -oxidation, and adipocyte browning in WAT of *Cpt1b*^{m−/−} mice. Moreover, expression of browning markers was reversed in iWAT of DKO mice, reaching levels similar to those in control mice. However, the reversal of browning markers has no effect on fat mass as measured by NMR, mass of individual fat depots, or adipocyte histology, suggesting the level of browning observed in *Cpt1b*^{m−/−} mice is not high enough to increase whole-body energy expenditure. The lack of an effect of FGF21 on adiposity was also observed in the transgenic mice overexpressing UCP-1 in skeletal muscle (Ost et al., 2015).

In summary, the combination of elevated fatty acids and CPT1b inhibition increases FGF21 production in skeletal muscle via an AMPK-mTor-Akt1 pathway. This regulation does not involve induction of the ER stress pathway, which has been reported to be a primary mediator of FGF21 induction in skeletal muscle under pathological conditions. Results from the present study indicate that production of FGF21 in skeletal muscle of *Cpt1b*^{m−/−} mice improves metabolic health, because FGF21 appears to act in a paracrine manner in muscle to improve glucose uptake in these mice. While circulating FGF21 does produce browning in adipose tissue, FGF21 does not drive the obesity-resistant phenotype observed in *Cpt1b*^{m−/−} mice. Further studies are needed to evaluate FGF21-independent pathways in *Cpt1b*^{m−/−} mice that would provide new insights on resistance to diet-induced obesity. Altogether, our findings suggest that pharmacologically targeted CPT1b inhibition specifically in skeletal muscle could trigger favorable adaptive responses, resulting in improved glucose uptake and reduced fat mass, and that the improvements in glucose homeostasis are partially driven by muscle-specific upregulation of FGF21.

EXPERIMENTAL PROCEDURES

Animal Studies

Animal studies were conducted at Pennington Biomedical Research Center's American Association for Laboratory Animal Care (AALAC)-approved facility on a standard breeder chow diet, composed of 20% protein, 25% fat, and 55% carbohydrate (Purina Rodent Chow no. 5015, Purina Mills). All experiments were in compliance with the NIH Guide for the Care and Use of Laboratory Animals and approved by the Institutional Animal Care and Use Committee. All mice used in the experiments were 3–4 months old unless specified otherwise.

Animal Procedures

Serum and plasma collections were performed by submandibular bleed. GTTs were performed following a 4-hr fast by intraperitoneal (i.p.) injection of 10% D-glucose (0.68 g/kg body weight). ITTs were done in the fed state using an i.p. dose of 0.04 U/kg body weight. For insulin signaling studies, mice were fasted overnight and then given an i.p. injection of insulin (1.0 U/kg body

weight); tissues were collected 10 min later. Indirect calorimetry was done in a 16-chamber Oxymax system (Columbus Instruments) (Wicks et al., 2015).

ELISA

ELISA kits were used for measurement of FGF21 (BioVendor) in serum and supernatant of mouse primary muscle cell culture, IGF-1 (Abcam) in serum, and total and high molecular weight adiponectin (ALPCO Diagnostics) in plasma.

qRT-PCR

qRT-PCR was conducted using $\Delta\Delta C_T$ assay as described previously (Vandanmagsar et al., 2011). Mouse and human cyclophilin B were used as a house-keeping-gene control for normalization of gene expression. Primer details are provided in Table S1.

Western Blot Analysis

Protein homogenates were prepared from muscle tissue in cell lysis buffer (EMD Millipore). Immunoblot analyses were performed using standard procedures. See Supplemental Experimental Procedures for details.

Mouse Primary Muscle Cell Culture

Cultures were established from mixed hindlimb muscle from 1- and 3- to 5-month-old *Cpt1b*^{m-/-} and *Cpt1b*^{fl/fl} littermates (Rando and Blau, 1994). See Supplemental Experimental Procedures for details.

Human Skeletal Muscle Myoblast Culture

Cryopreserved human skeletal muscle myoblasts (HSMs) from four normal-lean (BMI, 19.8 ± 0.7), and four diabetic-obese (BMI, 32.6 ± 4.2) subjects at passage 2 were purchased from Lonza and cultured as previously described (Vandanmagsar et al., 2014). See Supplemental Experimental Procedures for details.

Multiplex Mapmate Signaling Assay

Harvested muscle tissue from mouse was snap-frozen in liquid nitrogen. Then, entire muscle tissue was powdered in liquid nitrogen and used for protein lysate preparation in cell signaling lysis buffer (Millipore). Differentiated and treated human myotubes were harvested in cell signaling lysis buffer (Millipore). See Supplemental Experimental Procedures for details.

Glucose Uptake

Glucose uptake was measured in mouse primary myotubes as described in Noland et al. (2009). See Supplemental Experimental Procedures for details.

Substrate Oxidation Assays

Gastrocnemius muscle homogenates were prepared as previously described (Noland et al., 2007). Peroxisomal FAO was measured from [1-¹⁴C]lignoceric acid (20 μM), PDH activity and pyruvate oxidation were measured from [1-¹⁴C]pyruvate and [3-¹⁴C]pyruvate, and leucine oxidation was measured by capturing ¹⁴CO₂ from [U-¹⁴C]leucine (100 μM) as previously described (Wicks et al., 2015).

Statistical Analysis

Data are expressed as mean ± SEM. GraphPad Prism 5 software was used for ANOVA or repeated-measures ANOVA and Bonferroni post-tests or two-tailed Student's t test. p < 0.05 was considered significant.

SUPPLEMENTAL INFORMATION

Supplemental Information includes Supplemental Experimental Procedures, seven figures, and one table and can be found with this article online at <http://dx.doi.org/10.1016/j.celrep.2016.04.057>.

AUTHOR CONTRIBUTIONS

Data Collection and Manuscript Preparation, B.V., J.D.W., S.E.W., R.C.N., and R.L.M.; Data Analysis, S.G. and J.M.S.; Histology, D.B.; Technical Assistance, O.S.D., T.M.M., and J.Z.

ACKNOWLEDGMENTS

This work used PBRC core facilities that are supported in part by COBRE (NIH 8 P20-GM103528) and NORC (NIH 2P30-DK072476) center grants from the NIH. This research was supported by ADA grant 1-10-BS-129 and NIH grant R01DK089641 to R.L.M. R.C.N. is supported by R01DK103860. J.D.W. is supported by T32 fellowship T32DK6458413. This work was also supported in part by NIH grant 1U54-GM-104940, which funds the Louisiana Clinical and Translational Science Center.

Received: January 4, 2016

Revised: March 7, 2016

Accepted: April 14, 2016

Published: May 12, 2016

REFERENCES

- Badman, M.K., Pissios, P., Kennedy, A.R., Koukos, G., Flier, J.S., and Maratos-Flier, E. (2007). Hepatic fibroblast growth factor 21 is regulated by PPARα and is a key mediator of hepatic lipid metabolism in ketotic states. *Cell Metab.* 5, 426–437.
- Badman, M.K., Koester, A., Flier, J.S., Kharitonov, A., and Maratos-Flier, E. (2009). Fibroblast growth factor 21-deficient mice demonstrate impaired adaptation to ketosis. *Endocrinology* 150, 4931–4940.
- Bookout, A.L., de Groot, M.H., Owen, B.M., Lee, S., Gautron, L., Lawrence, H.L., Ding, X., Elmquist, J.K., Takahashi, J.S., Mangelsdorf, D.J., and Kliewer, S.A. (2013). FGF21 regulates metabolism and circadian behavior by acting on the nervous system. *Nat. Med.* 19, 1147–1152.
- Brahma, M.K., Adam, R.C., Pollak, N.M., Jaeger, D., Zierler, K.A., Pöcher, N., Schreiber, R., Romauch, M., Moustafa, T., Eder, S., et al. (2014). Fibroblast growth factor 21 is induced upon cardiac stress and alters cardiac lipid homeostasis. *J. Lipid Res.* 55, 2229–2241.
- Brooks, G.A. (1997). Importance of the “crossover” concept in exercise metabolism. *Clin. Exp. Pharmacol. Physiol.* 24, 889–895.
- Brooks, G.A., and Mercier, J. (1994). Balance of carbohydrate and lipid utilization during exercise: the “crossover” concept. *J. Appl. Physiol.* 76, 2253–2261.
- Chen, W.S., Xu, P.Z., Gottlob, K., Chen, M.L., Sokol, K., Shiyanova, T., Roninson, I., Weng, W., Suzuki, R., Tobe, K., et al. (2001). Growth retardation and increased apoptosis in mice with homozygous disruption of the Akt1 gene. *Genes Dev.* 15, 2203–2208.
- Chiang, G.G., and Abraham, R.T. (2005). Phosphorylation of mammalian target of rapamycin (mTOR) at Ser-2448 is mediated by p70S6 kinase. *J. Biol. Chem.* 280, 25485–25490.
- Chong-Kopera, H., Inoki, K., Li, Y., Zhu, T., Garcia-Gonzalo, F.R., Rosa, J.L., and Guan, K.L. (2006). TSC1 stabilizes TSC2 by inhibiting the interaction between TSC2 and the HERC1 ubiquitin ligase. *J. Biol. Chem.* 281, 8313–8316.
- Copps, K.D., and White, M.F. (2012). Regulation of insulin sensitivity by serine/threonine phosphorylation of insulin receptor substrate proteins IRS1 and IRS2. *Diabetologia* 55, 2565–2582.
- Coskun, T., Bina, H.A., Schneider, M.A., Dunbar, J.D., Hu, C.C., Chen, Y., Molter, D.E., and Kharitonov, A. (2008). Fibroblast growth factor 21 corrects obesity in mice. *Endocrinology* 149, 6018–6027.
- Dagenais, G.R., Tancredi, R.G., and Zierler, K.L. (1976). Free fatty acid oxidation by forearm muscle at rest, and evidence for an intramuscular lipid pool in the human forearm. *J. Clin. Invest.* 58, 421–431.
- De Sousa-Coelho, A.L., Marrero, P.F., and Haro, D. (2012). Activating transcription factor 4-dependent induction of FGF21 during amino acid deprivation. *Biochem. J.* 443, 165–171.
- Ferré, P. (2004). The biology of peroxisome proliferator-activated receptors: relationship with lipid metabolism and insulin sensitivity. *Diabetes (Suppl 1)*, S43–S50.
- Fisher, F.M., Kleiner, S., Douris, N., Fox, E.C., Mepani, R.J., Verdegue, F., Wu, J., Kharitonov, A., Flier, J.S., Maratos-Flier, E., and Spiegelman, B.M.

- (2012). FGF21 regulates PGC-1 α and browning of white adipose tissues in adaptive thermogenesis. *Genes Dev.* 26, 271–281.
- Fon Tacer, K., Bookout, A.L., Ding, X., Kurosu, H., John, G.B., Wang, L., Goetz, R., Mohammadi, M., Kuro-o, M., Mangelsdorf, D.J., and Kliewer, S.A. (2010). Research resource: comprehensive expression atlas of the fibroblast growth factor system in adult mouse. *Mol. Endocrinol.* 24, 2050–2064.
- Garofalo, R.S., Orena, S.J., Rafidi, K., Torchia, A.J., Stock, J.L., Hildebrandt, A.L., Coskran, T., Black, S.C., Brees, D.J., Wicks, J.R., et al. (2003). Severe diabetes, age-dependent loss of adipose tissue, and mild growth deficiency in mice lacking Akt2/PKB beta. *J. Clin. Invest.* 112, 197–208.
- Goodpaster, B.H., He, J., Watkins, S., and Kelley, D.E. (2001). Skeletal muscle lipid content and insulin resistance: evidence for a paradox in endurance-trained athletes. *J. Clin. Endocrinol. Metab.* 86, 5755–5761.
- Gorentla, B.K., Wan, C.K., and Zhong, X.P. (2011). Negative regulation of mTOR activation by diacylglycerol kinases. *Blood* 117, 4022–4031.
- Guridi, M., Tintignac, L.A., Lin, S., Kupr, B., Castets, P., and Rüegg, M.A. (2015). Activation of mTORC1 in skeletal muscle regulates whole-body metabolism through FGF21. *Sci. Signal.* 8, ra113.
- Harris, L.A., Skinner, J.R., Shew, T.M., Pietka, T.A., Abumrad, N.A., and Wolins, N.E. (2015). Perilipin 5-driven lipid droplet accumulation in skeletal muscle stimulates the expression of fibroblast growth factor 21. *Diabetes* 64, 2757–2768.
- Haynes, C.M., and Ron, D. (2010). The mitochondrial UPR—protecting organelle protein homeostasis. *J. Cell Sci.* 123, 3849–3855.
- Hojman, P., Pedersen, M., Nielsen, A.R., Krogh-Madsen, R., Yfanti, C., Akerstrom, T., Nielsen, S., and Pedersen, B.K. (2009). Fibroblast growth factor-21 is induced in human skeletal muscles by hyperinsulinemia. *Diabetes* 58, 2797–2801.
- Holland, W.L., Adams, A.C., Brozinick, J.T., Bui, H.H., Miyauchi, Y., Kusminski, C.M., Bauer, S.M., Wade, M., Singhal, E., Cheng, C.C., et al. (2013). An FGF21-adiponectin-ceramide axis controls energy expenditure and insulin action in mice. *Cell Metab.* 17, 790–797.
- Hotta, Y., Nakamura, H., Konishi, M., Murata, Y., Takagi, H., Matsumura, S., Inoue, K., Fushiki, T., and Itoh, N. (2009). Fibroblast growth factor 21 regulates lipolysis in white adipose tissue but is not required for ketogenesis and triglyceride clearance in liver. *Endocrinology* 150, 4625–4633.
- Huang, J., and Manning, B.D. (2008). The TSC1-TSC2 complex: a molecular switchboard controlling cell growth. *Biochem. J.* 412, 179–190.
- Huang, J., and Manning, B.D. (2009). A complex interplay between Akt, TSC2 and the two mTOR complexes. *Biochem. Soc. Trans.* 37, 217–222.
- Inagaki, T., Dutchak, P., Zhao, G., Ding, X., Gautron, L., Parameswara, V., Li, Y., Goetz, R., Mohammadi, M., Esser, V., et al. (2007). Endocrine regulation of the fasting response by PPAR α -mediated induction of fibroblast growth factor 21. *Cell Metab.* 5, 415–425.
- Inagaki, T., Lin, V.Y., Goetz, R., Mohammadi, M., Mangelsdorf, D.J., and Kliewer, S.A. (2008). Inhibition of growth hormone signaling by the fasting-induced hormone FGF21. *Cell Metab.* 8, 77–83.
- Inoki, K., Zhu, T., and Guan, K.L. (2003). TSC2 mediates cellular energy response to control cell growth and survival. *Cell* 115, 577–590.
- Izumiya, Y., Bina, H.A., Ouchi, N., Akasaki, Y., Kharitonov, A., and Walsh, K. (2008). FGF21 is an Akt-regulated myokine. *FEBS Lett.* 582, 3805–3810.
- Keipert, S., Ost, M., Johann, K., Imber, F., Jastroch, M., van Schothorst, E.M., Keijer, J., and Klaus, S. (2014). Skeletal muscle mitochondrial uncoupling drives endocrine cross-talk through the induction of FGF21 as a myokine. *Am. J. Physiol. Endocrinol. Metab.* 306, E469–E482.
- Kelley, D.E., Mokan, M., Simoneau, J.A., and Mandarino, L.J. (1993). Interaction between glucose and free fatty acid metabolism in human skeletal muscle. *J. Clin. Invest.* 92, 91–98.
- Kharitonov, A., Shivanova, T.L., Koester, A., Ford, A.M., Micanovic, R., Galbreath, E.J., Sandusky, G.E., Hammond, L.J., Moyers, J.S., Owens, R.A., et al. (2005). FGF-21 as a novel metabolic regulator. *J. Clin. Invest.* 115, 1627–1635.
- Kim, D.H., Sarbassov, D.D., Ali, S.M., King, J.E., Latek, R.R., Erdjument-Bromage, H., Tempst, P., and Sabatini, D.M. (2002). mTOR interacts with raptor to form a nutrient-sensitive complex that signals to the cell growth machinery. *Cell* 110, 163–175.
- Kim, K.H., Jeong, Y.T., Kim, S.H., Jung, H.S., Park, K.S., Lee, H.Y., and Lee, M.S. (2013a). Metformin-induced inhibition of the mitochondrial respiratory chain increases FGF21 expression via ATF4 activation. *Biochem. Biophys. Res. Commun.* 440, 76–81.
- Kim, K.H., Jeong, Y.T., Oh, H., Kim, S.H., Cho, J.M., Kim, Y.N., Kim, S.S., Kim, D.H., Hur, K.Y., Kim, H.K., et al. (2013b). Autophagy deficiency leads to protection from obesity and insulin resistance by inducing Fgf21 as a mitokine. *Nat. Med.* 19, 83–92.
- Kolumam, G., Chen, M.Z., Tong, R., Zavala-Solorio, J., Kates, L., van Bruggen, N., Ross, J., Wyatt, S.K., Gandham, V.D., Carano, R.A., et al. (2015). Sustained brown fat stimulation and insulin sensitization by a humanized bispecific antibody agonist for fibroblast growth factor receptor 1/ β Klotho complex. *EBioMedicine* 2, 730–743.
- Lee, M.S., Choi, S.E., Ha, E.S., An, S.Y., Kim, T.H., Han, S.J., Kim, H.J., Kim, D.J., Kang, Y., and Lee, K.W. (2012). Fibroblast growth factor-21 protects human skeletal muscle myotubes from palmitate-induced insulin resistance by inhibiting stress kinase and NF- κ B. *Metabolism* 61, 1142–1151.
- Ma, L., Chen, Z., Erdjument-Bromage, H., Tempst, P., and Pandolfi, P.P. (2005). Phosphorylation and functional inactivation of TSC2 by Erk implications for tuberous sclerosis and cancer pathogenesis. *Cell* 121, 179–193.
- Mashili, F.L., Austin, R.L., Deshmukh, A.S., Fritz, T., Caidahl, K., Bergdahl, K., Zierath, J.R., Chibalin, A.V., Moller, D.E., Kharitonov, A., and Krook, A. (2011). Direct effects of FGF21 on glucose uptake in human skeletal muscle: implications for type 2 diabetes and obesity. *Diabetes Metab. Res. Rev.* 27, 286–297.
- Nabben, M., Hoeks, J., Moonen-Kornips, E., van Beurden, D., Briedé, J.J., Hesselink, M.K., Glatz, J.F., and Schrauwen, P. (2011). Significance of uncoupling protein 3 in mitochondrial function upon mid- and long-term dietary high-fat exposure. *FEBS Lett.* 585, 4010–4017.
- Nishimura, T., Nakatake, Y., Konishi, M., and Itoh, N. (2000). Identification of a novel FGF, FGF-21, preferentially expressed in the liver. *Biochim. Biophys. Acta* 1492, 203–206.
- Noland, R.C., Woodlief, T.L., Whitfield, B.R., Manning, S.M., Evans, J.R., Dudek, R.W., Lust, R.M., and Cortright, R.N. (2007). Peroxisomal-mitochondrial oxidation in a rodent model of obesity-associated insulin resistance. *Am. J. Physiol. Endocrinol. Metab.* 293, E986–E1001.
- Noland, R.C., Koves, T.R., Seiler, S.E., Lum, H., Lust, R.M., Ilkayeva, O., Stevens, R.D., Hegardt, F.G., and Muoio, D.M. (2009). Carnitine insufficiency caused by aging and overnutrition compromises mitochondrial performance and metabolic control. *J. Biol. Chem.* 284, 22840–22852.
- Ogawa, Y., Kurosu, H., Yamamoto, M., Nandi, A., Rosenblatt, K.P., Goetz, R., Eliseenkova, A.V., Mohammadi, M., and Kuro-o, M. (2007). BetaKlotho is required for metabolic activity of fibroblast growth factor 21. *Proc. Natl. Acad. Sci. USA* 104, 7432–7437.
- Ost, M., Coleman, V., Voigt, A., van Schothorst, E.M., Keipert, S., van der Stelt, I., Ringel, S., Graja, A., Ambrosi, T., Kipp, A.P., et al. (2015). Muscle mitochondrial stress adaptation operates independently of endogenous FGF21 action. *Mol. Metab.* 5, 79–90.
- Rando, T.A., and Blau, H.M. (1994). Primary mouse myoblast purification, characterization, and transplantation for cell-mediated gene therapy. *J. Cell Biol.* 125, 1275–1287.
- Suomalainen, A., Elo, J.M., Pietiläinen, K.H., Hakonen, A.H., Sevastianova, K., Korpela, M., Isohanni, P., Marjavaara, S.K., Tyni, T., Kiuru-Enari, S., et al. (2011). FGF-21 as a biomarker for muscle-manifesting mitochondrial respiratory chain deficiencies: a diagnostic study. *Lancet Neurol.* 10, 806–818.
- Tyynismaa, H., Carroll, C.J., Raimundo, N., Ahola-Erkkilä, S., Wenz, T., Ruhanen, H., Guse, K., Hemminki, A., Peltola-Mjøsund, K.E., Tulkkki, V., et al. (2010). Mitochondrial myopathy induces a starvation-like response. *Hum. Mol. Genet.* 19, 3948–3958.

- Um, S.H., Frigerio, F., Watanabe, M., Picard, F., Joaquin, M., Sticker, M., Fumagalli, S., Allegrini, P.R., Kozma, S.C., Auwerx, J., and Thomas, G. (2004). Absence of S6K1 protects against age- and diet-induced obesity while enhancing insulin sensitivity. *Nature* *431*, 200–205.
- Vandanmagsar, B., Youm, Y.H., Ravussin, A., Galgani, J.E., Stadler, K., Mynatt, R.L., Ravussin, E., Stephens, J.M., and Dixit, V.D. (2011). The NLRP3 inflammasome instigates obesity-induced inflammation and insulin resistance. *Nat. Med.* *17*, 179–188.
- Vandanmagsar, B., Haynie, K.R., Wicks, S.E., Bermudez, E.M., Mendoza, T.M., Ribnicky, D., Cefalu, W.T., and Mynatt, R.L. (2014). *Artemisia dracunculoides* L. extract ameliorates insulin sensitivity by attenuating inflammatory signaling in human skeletal muscle culture. *Diabetes Obes. Metab.* *16*, 728–738.
- Wicks, S.E., Vandanmagsar, B., Haynie, K.R., Fuller, S.E., Warfel, J.D., Stephens, J.M., Wang, M., Han, X., Zhang, J., Noland, R.C., and Mynatt, R.L. (2015). Impaired mitochondrial fat oxidation induces adaptive remodeling of muscle metabolism. *Proc. Natl. Acad. Sci. USA* *112*, E3300–E3309.
- Wouters, B.G., and Koritzinsky, M. (2008). Hypoxia signalling through mTOR and the unfolded protein response in cancer. *Nat. Rev. Cancer* *8*, 851–864.
- Wulschleger, S., Loewith, R., and Hall, M.N. (2006). TOR signaling in growth and metabolism. *Cell* *124*, 471–484.
- Xu, H., Hertzler, A.V., Steen, K.A., Wang, Q., Suttles, J., and Bernlohr, D.A. (2015). Uncoupling lipid metabolism from inflammation through fatty acid binding protein-dependent expression of UCP2. *Mol. Cell. Biol.* *35*, 1055–1065.